CFD MODELLING OF AN INITIAL POWDERY LAYER ON COOLED TUBULAR SURFACES

***J. Strouhal[1], T. Juřena, and Z. Jegla**
[1] Brno University of Technology, Faculty of Mechanical Engineering, Institute of Process Engineering, Technická 2896/2, 616 69 Brno, Czech Republic. E-mail: Jiri.Strouhal@vutbr.cz

ABSTRACT
Fouling in convective parts of boilers is typical of the deposition of solid particles and condensable inorganic vapours. Particle sticking is caused mainly by gravity, adhesion, or the presence of a sticky liquid film of condensed vapours. Aside from the local conditions, particle properties and size determine whether they are sticking on the surface. This work focuses on simulations of particulate matter fouling of cooled tubes by fly ash produced by the combustion of industrial waste and sewage sludge mixture. Boundary conditions including the flue gas and particle flow rate are derived from combustion tests. Particle properties and size distribution are obtained from literature. The goal is to provide a basis for further CFD modelling of the development of large deposits in tube bundles observed during a test on the experimental facility. Neither the combustion nor fly ash development is modelled. Their transport and deposition are simulated. Fixed boundary conditions are set for both the particulate and gas phases. The influence of already deposited particles on the surface mechanical properties and roughness is included to capture their deposition. The fly ash particles are considered completely solidified, considering the the low flue gas temperatures on the facility inlet.

INTRODUCTION
Particulate matter (PM) fouling occurs during co-combustion of solid alternative fuels such as industrial waste, sewage sludge, and woody biomass. It causes a decrease in efficiency, reliability, and safety of operation of the whole facility by affecting the heat transfer efficiency, pressure loss, and local temperature of both the cooling media and the flue gas. For detailed analysis, simulations of the local conditions on (not only) the heat transfer surfaces enable to predict possible operational problems, their location, and the period, after which they occur.

Instead of using empirical indices giving information about the overall behaviour of fuels, individual mechanisms occurring in the boiler can be analysed, including production, transport and deposition of combustion products, and possible erosion of created deposits [1]. For each of these processes, a standalone model can be created. Computational Fluid Dynamics (CFD) can be used to model all these individual processes and their interactions. Detailed modelling of the fouling sub-processes instead of the global process is useful namely in the case of using highly heterogeneous fuels such as municipal solid waste [2].

This work intends to extend the previous work of Strouhal et al. [3]. The fly ash sticking model (described in further sections) was so far tested for the relative significance of its parameters, e.g., the particle surface energy. Other works on the topic of PM fouling contain models for particle transport, sticking and rebound. Here, those suitable for the investigated case are selected and combined (e.g., the model for particle sticking [4] or the influence of the surface roughness [5]).

Here, the model is applied to a case of cooled tube bundles inside an experimental heat exchanger, having maximum inlet temperatures of 300 to 400 °C. In the presence of volatile inorganic components, coated particles can be expected to be produced, changing their sticking behaviour in contrast to clean fly ash. At the start of the fouling process, the tube bundle geometry is still not changed significantly. However, the surface structure does change due to the presence of deposited fly ash particles, which affects the fouling rate. Using the data from the experimental facility, these effects were examined.

MODELLING OF FLY ASH STICKING ON COOLED SURFACES
Lee et al. [6] provide a model for the simulation of ash particles covered by viscous film impacting the cooled tubes covered by a powdery deposit. It is a combination of both the viscosity-based and velocity-based sticking models. Flue gas and fly ash properties are set as boundary conditions, using data from industrial boilers.

The development of the liquid sticky layer on the particle surfaces in [6] is estimated from the local conditions and the condensable vapour concentration. The data used for the model include

ISBN: 978-0-9984188-2-7; Published online www.heatexchanger-fouling.com

overall fly ash load, flue gas temperature, the geometry of the fouled surfaces and sodium contents in the fuel, which represented the amount of the condensable vapours. Inertial impaction is explicitly chosen as the only assumed impaction mechanism and neglects other phenomena, which might influence the large particle deposition, such as turbulent dispersion [7].

Cooled surfaces

To design a new arrangement of tubes in a bundle in the heat recovery device, Li et al. [8] used their fouling model. In this model, thermophoresis, Brownian motion, and Saffman's lift are introduced into the particle motion model. The particle is assumed to impact a smooth surface. No changes in the impaction direction are introduced. Adhesion, external forces, and plastic deformation are assumed to cause a decrease in momentum in the normal direction. For tangential direction, momentum balance with net sink is also assumed. No expressions for these losses are stated explicitly; the authors refer to the work of Brach and Dunn [9]. The wall friction velocity is used for the determination of particles sticking to the wall via the momentum balance of the impacting particle.

Sticky wall model

Condensation of inorganic vapours occurs on the deposit or wall surface and contributed to the overall sticking probability [10]. This leads to additional terms in the sticking probability estimation. In the case of a model from the group of *critical* models, where the probability is either 0 or 1, this additional contribution effectively shifts the critical value. Lee et al. [6] assume heterogeneous condensation on the surfaces.

$$P = P_p + \left(1 - P_p\right) P_s - k_e \left(1 - P_p\right)(1 - P_s) \quad (1)$$

The P_p and P_s are the particle and surface sticking probability contributions. The overall sticking probability is given by contribution from sticky particles, then from sticky surface capturing non-sticky particles. The last term having a negative sign represents the erosion of the deposit due to the impaction of non-sticky particles to the non-sticky surface and such impacts can lead to deposit erosion. In this model, the influence of various mechanical properties and local conditions is represented by a parameter k_e. Hansen et al. [10] neglect the erosion by choosing $k_e = 0$.

Particle sticking probability

The particle sticking probability is determined by a critical velocity model, judging the magnitude of the impact velocity normal component. The used model is identical to the one developed by Thornton and Ning [4] for adhesive elastic particles impacting smooth flat surfaces.

It is not explicitly stated, if the particles are sticky due to pure adhesion between their solid surface and the non-sticky wall or if there is an additional effect, e.g., due to the presence of a condensed layer on the particle. The surface energy used in the critical velocity calculation might represent both such situations. Calculation of surface energy of the multi-component system, e.g., particle-liquid, film-wall, is described by Losurdo et al. [11]

Deposit surface sticking probability

The sticking probability contribution from a sticky surface is determined aside from the surface tension by the surface orientation and the surface layer viscosity. Note, that this model enables non-sticky particles to deposit only on surfaces pointing upwards, thus no such deposition occurs on walls (smooth) or ceilings.

Effect of the deposit surface temperature

To determine the local conditions properly and to account for the cooling at heat transfer surfaces, the following must be determined:
- temperature of the cooling media,
- heat transfer coefficient at the cooling media side,
- thermal conductivity of the wall,
- thermal conductivity of the deposit,
- surface roughness of the deposit, affecting the heat transfer coefficient on the flue gas side.

Hansen et al. [10] used the estimation of the effective deposit conductivity, which was developed and validated originally by Sugawara and Yoshizawa [12].

Aside from the influence of the deposit pores, their model introduces additional parameters for capturing the effect of the pores' shape by using a modified void fraction in the weighted averaging of the thermal conductivity. Further sintering increases the overall effective conductivity by increasing the contact surface area between individual particles. Example of modelling this effect can be found in [13].

Surface tension of particle surface layer

Lee et al. [6] used the surface tension of a specific salt, that was assumed to condense on a surface of particles. Two cases of adhesion can be distinguished, with and without contact with solid surfaces. The particle is assumed to be captured by the viscous layer without the solid-solid contact even occurring.

In the case of solid-solid contact, the adhesion will be a result of both types of contact. The surface tension of various molten compounds, e.g., Na_2O, K_2O and their temperature dependencies are summarized by Kleinhans et al. [1]. KCl surface energy at 25 °C can be found in [14].

ISBN: 978-0-9984188-2-7; Published online www.heatexchanger-fouling.com

Condensed layer melting behaviour

Kaer at al. [15] present melting behaviour of KCl and SiO_2, as well as melting behaviour of fly ash, collected in a convective part of a straw-fired boiler. These are depicted for temperatures 0 to 1400 °C. Silica melting behaviour is not among the objectives as the melted fraction occurs at temperatures higher than 900 °C, which is above temperatures observed in the fouled part of the whole modelled facility.

Effect of the surface roughness

Particle and wall surface roughness leads to several effects: deviation in the rebound direction, changes in the effective mechanical properties, caused by deformation or even breakup of the impacted part of the deposit, and multiple impactions, leading to increased damping of the impactor's motion.

Sommerfeld and Huber [16] developed a model accounting for the deviation in the rebound velocity in both the tangential and transversal directions. The authors introduce a random deviation to the surface normal vector, based on a known surface roughness The model also accounts for a so-called *shadow effect*. if the virtual surface's normal vector points away from the impacting particle and thus, a collision with this virtual surface cannot occur.

MATHEMATICAL MODEL

Sticking model

The following model was used in the previous work [3]. The particle sticking to the surface is modelled using a combination of models of the normal impaction of elastic-perfectly plastic, adhesive spheres on a flat surface [4] and a model for the oblique impact of fly ash particles [17].

The normal impact model provides a value of a normal restitution coefficient for determining if the particle sticks to the wall. The effective Young's modulus E^*, yield limit y, and the contact surface energy γ for the particle-surface system are used as the model inputs, aside from the particle density and size. Expressions for the E^* and y are given in [4]. During the particle-surface collision, the particle rebounds with smaller kinetic energy compared to the state before impaction. For small impaction velocities, elastic waves occur in the wall or deposit material, carrying away part of the energy. If the kinetic energy regained by the particle during returning to its original shape (assuming only elastic deformation) is too low, the particle cannot overcome the adhesion to the surface and remains stuck to the surface. A minimum normal impaction velocity v_s is required (Eq(2)).

$$v_s = 1.84 \left(\frac{2\gamma}{d_p}\right)^{\frac{5}{6}} \Big/ \left(\rho_p^3 E^{*2}\right)^{\frac{1}{6}} \quad (2)$$

The ρ_p is the particle density and d_p its diameter. If the impaction velocity is high enough, the plastic deformation of the particle is assumed to occur, as expressed with Eq(3).

$$v_y = 1.56 \left[\frac{y_S^5}{\rho_p^3 E^{*2}}\right]^{0.5} \quad (3)$$

The two velocities are used for the calculation of the normal restitution coefficient (Eq(4)) [4].

$$e_n = v_{n,r}/v_{n,i} \quad (4)$$

The tangential component of the particle movement is solved assuming the e_n being independent of the impaction angle. Xie et al. [17] developed model for the tangential restitution coefficient e_t using experiments with fly ash with diameters 47 to 53 μm impacting a flat, smooth stainless steel at impaction angles 15 to 75°.

The effect of surface roughness

A model [16] is used to model the effect of a rough surface produced by deposited particles. It is also implemented in ANSYS Fluent via the Rough Wall Model [5]. This model requires inputs describing the roughness of the surface, which leads to the question of how the surface roughness, i.e., the normal vector deviation can be described using the information about deposited particle sizes.

Three parameters describe the surface roughness in both vertical and horizontal directions: Ra, Rq and Rs_m, defined in [5]. The wall profile should be then derived from a geometry of the surface consisting of packed particles and thus reflects the deposited particle size and shape. Here, the particles are assumed to be spherical. Using the definitions in [5], the parameters can be expressed from the particle sizes and deposited masses on a surface (Eq(4)–Eq(9)).

$$P_i = \dot{m}_i/m_{p,i} \quad (5)$$

$$L = \sum_{i=1}^{N} P_i \, d_{p,i} \quad (6)$$

$$Ra = \frac{\pi}{8\,L} \sum_{i=1}^{N} P_i \, d_{p,i}^2 \quad (7)$$

$$Rq = \left[\frac{1}{12\,L}\sum_{i=1}^{N} P_i \, d_{p,i}^3\right]^{0.5} \quad (8)$$

$$Rs_m = L/\sum_{i=1}^{N} P_i \quad (9)$$

$$P_i = \dot{m}_i/m_{p,i} \quad (10)$$

where P_i is the number of particles deposited per unit of time, $\dot{m}_i$ is the deposition mass of the *i*th fraction and $m_{p,i}$ is the mass of a single particle, L is the length of the sampling profile, and N is the number of PM fractions. Only the deviation in the impaction plane, defined by the impaction velocity and the original surface normal vector, was considered. The angle deviation according to Sommerfeld and Huber [16] has a normal distribution with zero mean. The standard deviation σ_γ is defined by Eq(10) [5].

ISBN: 978-0-9984188-2-7; Published online www.heatexchanger-fouling.com

$$\sigma_\gamma = \begin{cases} \operatorname{atan}\left(2\frac{Rq}{RS_m}\right) & if\ d_p < \frac{RS_m}{\sin\left(\operatorname{atan}\left(2\frac{Rq}{RS_m}\right)\right)} \\ \operatorname{atan}\left(2\frac{Ra}{RS_m}\right) & otherwise \end{cases} \quad (11)$$

MODELLED CASE

Experimental facility

A facility installed at the Institute of Process Engineering of the Brno University of Technology provided a model case for the following simulations, including the heat transfer surface geometry and boundary and operating conditions.

It consists of three main parts. The first is the rotary kiln, enabling continuous feeding of the tested solid fuel and supporting the process with a gas burner. From there, the flue gas continues through a so-called deposition chamber, where part of the particulate matter (PM) should deposit due to sudden changes in the flow direction and cross-area [3].

The flue gas then continues to a heat exchanger, consisting of the main channel, containing four-tube bundles and a bypass. Each of the four bundles in the main channel contains six parallel tubes, filled with cooling water.

Model geometry

Because of the requirement to use a very fine mesh for the tube bundles compared to the deposition chamber simulations, the heat exchanger longitudinal section was chosen as the model geometry, reducing the problem into two dimensions (Fig. 1). Such an approach is chosen for the preparation and testing of the fouling model.

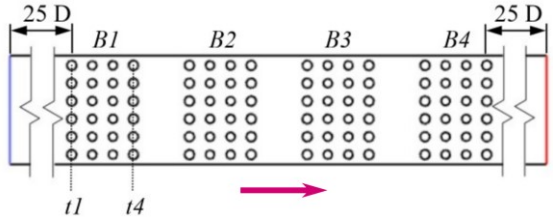

Fig. 1. Schematic representation of the model geometry; the red arrow shows the flow direction.

All four bundles were included in the model. The channel height was preserved. The distance of the inlet from the first bundle was set to 25 tube diameters ($D_{tube} = 26.9\,mm$). The same distance was used in the work [18] focused on the influence of the mesh and turbulence model on the predicted impaction rates. At the inlet, a line consisting of 1000 uniformly placed points was created, which will be used for the model particle injection.

Numerical model setup

Fluid flow model

The SST k-ω model was used for the simulation of the turbulent flow. The flue gas was modelled as ideal and non-compressible. Its molar mass, specific heat, thermal conductivity, and viscosity were based on a constant composition, which was determined from the mass balance of the combusted fuel and measured flue gas flow rate. The flow viscosity, thermal conductivity, and specific heat capacity were modelled as temperature- and composition-dependent, using relations for the ideal-gas mixture [5], data from [19] and the known composition of the flue gas (Table 1).

Table 1. Flue gas composition used for the inlet boundary condition calculation.

Gas	Mass fraction [%]
N_2	71.26
O_2	15.16
H_2O	5.99
CO_2	7.58

Based on the data measured during combustion tests in the experimental facility, boundary conditions were set including the inlet mass flow rate 0.138 kg/s and a temperature 315 °C. Turbulence intensity at the inlet was set to 4.9 % [5].

The water-cooled tubes were modelled using the temperature boundary condition. The waterside temperature was set according to the measured temperature of the feeding water and at the outlet of each of the four bundles. The sections of tubes in the 2D plane are grouped and labelled t1–t4 (same for each bundle), as shown in Fig. 1. The flue gas channel has a width 0.5 m.

Assuming the section plane to be the channel mid-plane and neglecting the length of the tube bends, each tube has a length of approximately 2 m. The flue gas temperature at these individual groups of tube sections is obtained from the feeding water temperature 23.8 °C and temperature at bundle outlets 37.2, 33.5, 31.7, and 29.9 °C, assuming approximately linear variation along each tube length. The temperatures in these sections are listed in Table 2.

Table 2. The temperature at the inner tube surfaces. The tube and bundle labelling is shown in Fig. 1.

T_w [°C]	t1	t2	t3	t4
B1	35.5	32.2	28.8	25.5
B2	32.3	29.9	27.4	25.0
B3	30.7	28.7	26.8	24.8
B4	29.1	27.6	26.1	24.6

The wall properties were set for the temperature 20 °C, using data for stainless steel from [20]. The tube wall thickness was set to 2.9 mm. The wall material properties are listed in Table 3.

Table 3. Input data for the convection model used on tube walls.

ρ_w [kg/m^3]	7850
λ_w [W/m K]	57
$c_{p,w}$ [J/kg K]	430

ISBN: 978-0-9984188-2-7; Published online www.heatexchanger-fouling.com

Particulate matter transport

The steady, Discrete Phase Model (DPM) is used for particle tracking. One-way coupling is used for all presented simulations, as the preliminary simulations did not show any observable effect on the flow field. The influence of the turbulent dispersion is modelled using the Discrete Random Walk (DRW) model, combined with the Random Eddy Lifetime model, with the Time Scale Constant set to 0.15. Note, that the DRW may give non-physical results for particles smaller few microns [5].

The thermophoretic force is included, although it is expected to significantly affect only those particles of diameter smaller than 10 μm [1]. Those particles include the smallest investigated PM fraction ($d_p = 6\ \mu m$). Effects of the virtual mass and pressure gradient forces are neglected, as they become significant only fluid-particle density ratio higher than 0.1 [5].

From the measured PM concentration before the heat exchanger inlet and the flue gas flow, the PM mass flow rate was calculated to be 11.1 mg/s. The particle size distribution (PSD) was obtained using data from the literature on the fluidized-bed combustion of municipal solid waste [21]. The average particle density was 2700 kg/m^3. The particles with $d_p > 100\ \mu m$ were not simulated; preliminary simulations have shown these are not able to leave the kiln. An average diameter d_p of each of the size ranges in [21] is used. The used PSD is represented by mass fractions y_i is contained in the Table 3.

Table 3. Fly ash PSD assumed at the exchanger inlet.

d_p [μm]	6	14	19.5	28.5	41.5	74.5
y_i [%]	44.6	7.6	8.0	9.3	10.4	20.0

Model implementation

ANSYS Fluent was used for the fouling simulations. The sticking model and rough wall model were implemented via User Defined Functions (UDF), consisting of C routines. Because the Rough Wall Model in the form implemented in Fluent support only constant roughness parameters, it had to be implemented as a part of the sticking model. For each of the impactions, the surface normal vector is tilted by an angle $\Delta\gamma$.

$$\Delta\gamma = \sigma_\gamma\ \zeta \tag{12}$$

ζ is a normally distributed random number having zero mean and standard deviation equal to one. In the UDF, the function *gauss_random()*, available from the Fluent function library, was used to generate ζ. To account for the *shadow effect* [16], the random try is repeated, if the dot product of the produced random normal vector and the impaction velocity vector is non-negative.

RESULTS AND DISCUSSION

Mesh comparison

The objective was to test the influence of mesh refinement in the tubes' vicinity. Two parameters were varied: the boundary cell height δ_0 and the number of nodes on tube circumference N_n, each affecting the obtained results. The outlet temperature T_{out} and the total deposition mass flow rate $\dot{m}_{dep}$ were observed. The boundary conditions were kept as described in previous sections. Sticking model parameters were set as $E^* = 50\ GPa$, $\gamma = 0.2\ N/m^2$, and $y_s = 500\ MPa$, as in [3].

The boundary cell height δ_1 at the tube wall was estimated using the Eq(11) and Eq(12) [18], where D_{tube} is the tube diameter, ρ_g is the gas density, $u_{g,\infty}$ is the gas free stream velocity and $\mu_{g,out}$ is the gas viscosity at temperature 153 °C, measured at the heat exchanger outlet.

$$\delta_1 = 0.324\ D_{tube}/Re_{tube}^{0.5} \tag{13}$$

$$Re_{tube} = \rho_g u_{g,\infty} D_{tube}/\mu_{g,out} \tag{14}$$

The δ_0 was computed as a fraction of the δ_1. Twelve generated meshes are listed in Table 4, along with the number of cells N_C, the average and maximum value of y^+ on tube walls. For better capturing of the $\dot{m}_{dep}$ variation, this quantity is shown in Fig. 2. The outlet temperature varied in a range of 3.4 °C around the average value 175.3 °C. Such a difference was considered negligible for the present work. Note, that the lowest value of δ_0 (31 μm) is smaller than the largest particle radius (37.5 μm) considered in the simulations. Particles with very small impaction angles can then be incorrectly considered to miss the wall surface, as its center does not enter the boundary cell layer, which is the condition for the particle to be considered as colliding with the wall.

Table 4. Parameters of the 12 tested meshes.

N_n	δ_0 [mm]	N_C	$\overline{y^+}$	y^+_{max}
48	0.248	127798	1.26	3.05
	0.124	136913	0.62	1.57
	0.062	154041	0.34	0.90
	0.031	170612	0.17	0.47
96	0.248	222459	1.25	3.06
	0.124	242275	0.65	1.70
	0.062	276604	0.34	0.91
	0.031	309203	0.17	0.47
192	0.248	474215	1.25	3.07
	0.124	526564	0.67	1.70
	0.062	580965	0.35	0.91
	0.031	644023	0.18	0.47

The mesh with $\delta_0 = 0.062\ mm$ and 96 nodes on the tube circumference was selected. This puts less computational requirements on subsequent simulations (namely in the case of the rough wall

ISBN: 978-0-9984188-2-7; Published online www.heatexchanger-fouling.com

model, where the boundary condition on roughness is obtained iteratively), by reducing the number of cells to half compared to the 192-node mesh with identical δ_0. The boundary cell height being $\delta_0 = \delta_1/4$ complies with the recommendation given by [18] for simulations of a cooled cylinder in a crossflow. As previously mentioned, choosing the lowest δ_0 might lead to underestimation of the deposition rate of the largest particles.

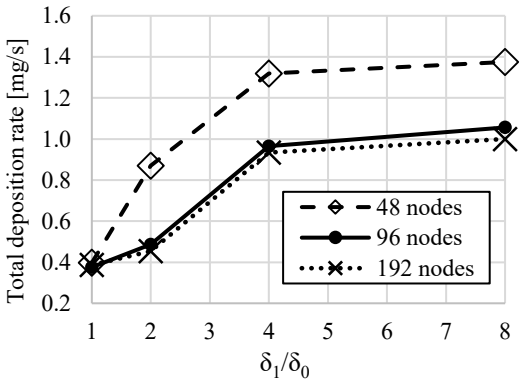

Fig. 2. Deposition mass flow rates obtained by varying δ_0 and N_n.

Effect of the roughness and particle coating

A further part of the work was to run simulations of cases with or without including an effect of a thick layer of condensed salt. In the simulation, the KCl was assumed to condense on the particle surfaces and the deposit and fouled surfaces. When hitting the tube surfaces, the particle's temperature is less than 315 °C, implying the KCl layer is completely solidified [15]. The properties of the clean and coated ash are shown in Table 5.

Table 5. Effective properties of clean and coated fly ash particles. Due to unavailable data, the yield strength was kept constant for both cases.

Property	Clean particles [21]	Particles strongly coated with KCl
γ [N/m^2]	0.13	0.11 [14]
E^* [GPa]	192	30 [1]
y_s [MPa]	38	38 [21]

For both cases of KCl presence, the effect of the roughness was tested. The roughness is estimated iteratively; the parameters Ra, Rq, and Rs_m are initially set to zero and after obtaining the deposition rates, they are updated, and the deposition rates are recalculated. Every location on the wall surface is either fully covered by deposited particles or clean. Including the surface roughness led to the increase of 30 % of the deposition rate for the clean surfaces, for the coated surfaces, the increase was 47.8 %. Fig. 4. shows positions with a very high change in the deposition mass flow rate. In the case of clean surfaces, the largest differences occur on the first tubes of the second bundle. Fig. 5 shows the two coarsest PM fractions to be the source of this increased deposition rate.

Table 6. Predicted deposition rates for surface properties variations.

$\dot{m}_{dep}$ [mg/s]	Smooth wall	Rough wall
Clean surfaces	2.071	2.692
Coated surfaces	1.102	1.629

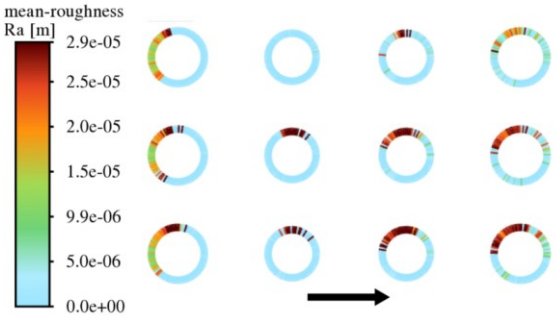

Fig. 3. Mean roughness height at the second, third, and fourth tube (bundle B1), counted from the exchanger's bottom. The arrow shows the flue gas flow direction.

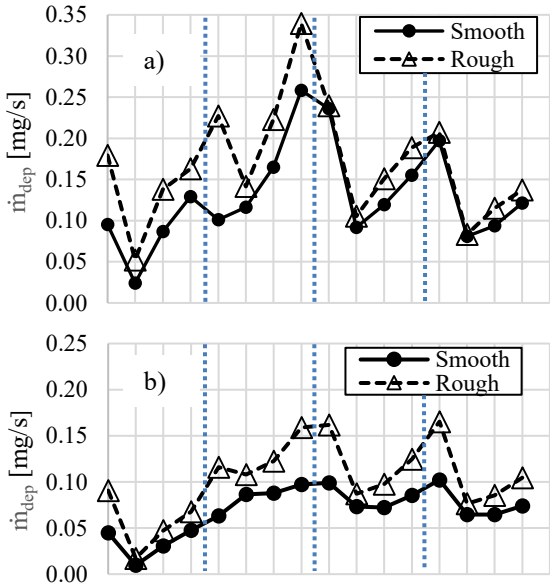

Fig. 4. Deposition rates at tube sections t1–t4 in the bundles B1–B2 for a) clean and b) coated surfaces. Dotted lines distinguish the individual bundles.

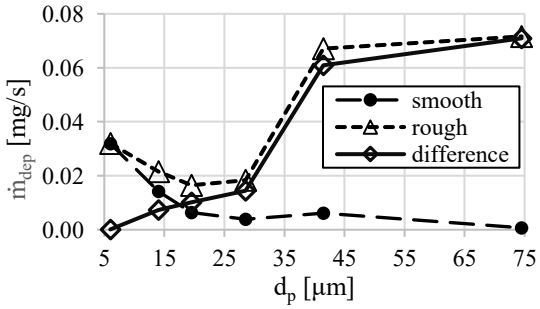

Fig. 5. Deposition rate per PM fraction at the first tubes of the second bundle (B2).

ISBN: 978-0-9984188-2-7; Published online www.heatexchanger-fouling.com

CONCLUSIONS

A CFD model of an initial deposit layer growth was proposed for the case of water-cooled tubes in the heat exchanger, which is part of the experimental facility for the investigation of the solid fuels' combustion process. The heat exchanger represents a region of relatively low temperature (315 °C at the inlet), compared to the deposition chamber and rotary kiln. Inertial impaction, turbulent dispersion and thermophoresis are used as the main ash deposition mechanisms. The particles are considered completely solidified and the condensation of inorganic vapours on particle surfaces is assumed to be already complete, considering the low temperature of the flue gas and intense mixing in the previous parts of the facility. Rough Wall Model present in the used software ANSYS Fluent [5] was modified and reimplemented to capture the effect of the initial layer of powdery layer on further deposition. The following conclusions can be made.

1. The mesh refinement near the tube wall vicinity must be sufficiently resolved. The boundary cell height must be equal to or smaller than 1/4 of the boundary layer displacement thickness to obtain a deposition rate with a relative error below 10 % (for the tested PSD), in compliance with the recommendations in [18]. The number of nodes placed on the tube circumference must be also set up sufficiently high, in this case at least 96.
2. Even in the case of a completely solidified layer of condensed vapours in a low-temperature region, the resulting deposition rate can be about 50 % lower compared to clean fly ash; in future work, emphasis will be taken on the prediction of the vapours affecting particle properties.
3. Including the surface roughness largely affects the predicted deposition rates of all the micron PM size fractions, and the overall deposition rate might increase more than 30 % over the smooth-surface model predictions. Note, that only the impaction angle was varied, without including the multiple impactions or changes in the impacted surface's mechanical properties.

NOMENCLATURE

c_p	Specific heat capacity, J/kg K
d, D	Diameter, m
e	Restitution coefficient, dimensionless
E^*	Effective Young modulus, Pa
k_e	erosivity, dimensionless
L	Sampling length, m
$\dot{m}_{dep}$	Total deposition mass flow rate, kg/s
N_C	Number of cells in a mesh, dimensionless
N_n	Number of nodes on tube circumference, dimensionless
P	Sticking probability, dimensionless; Deposited particles per unit time, s^{-1}
Ra	Wall mean roughness, m
Rq	Standard deviation of the roughness structure, m
RS_m	Mean profile element width or spacing, m
Re	Reynolds number, dimensionless
T_{out}	Outlet temperature, °C
T_w	Water temperature, °C
u	Velocity, m/s
v_s	Sticking velocity, m/s
v_y	Yield velocity, m/s
v	Particle velocity, m/s
y^+	Dimensionless distance
y_i	Mass fraction of *i*th particle size fraction, dimensionless
y_s	Static yield limit, Pa
γ	Specific surface energy, N/m^2
δ_0	Boundary cell height, m
δ_1	Boundary layer displacement thickness, m
$\Delta\gamma$	Random deviation of virtual wall angle, rad
ζ	Random number, dimensionless
λ	Thermal conductivity, W/m K
μ	Dynamic viscosity, Pa s
ρ	Density, kg/m^3
σ_γ	Standard deviation of the Gaussian distributed virtual wall angle, rad
CFD	Computational Fluid Dynamics
DPM	Discrete Phase Model
DRW	Discrete Random Walk
PM	Particulate matter
PSD	Particle Size Distribution
UDF	User Defined Functions

Subscripts

∞	free stream value
g	gas
i	impaction, summation index, species index
g	gas
max	maximum inside the computational domain
n	normal direction
out	flue gas outlet
p	particle
r	rebound
s	surface
t	tangential direction
tube	related to tube geometry
w	wall

ACKNOWLEDGEMENTS

The authors gratefully acknowledge the financial support provided by the Technology Agency of the Czech Republic (TACR) within the research project National Centers of Competence, specifically through the project National Centre for Energy (TN1000007).

REFERENCES

[1] Kleinhans, U., Wieland, Ch., Frandsen, F. J., and Spliethoff, H., *Ash formation and deposition in coal and biomass fired combustion systems: Progress and challenges in the field of ash particle sticking and rebound behavior*, Progress in Energy and Combustion Science. 2018, 68, 65–168. ISSN 0360-1285.

[2] Bryers, R. W., *Fireside slagging, fouling, and high-temperature corrosion of heat-transfer surface due to impurities in steam-raising fuels*, Progress in Energy and Combustion Science, 1996, 22(1), 29–120. ISSN 0360-1285.

[3] Strouhal, J., Juřena, T., and Jegla Z., *Fouling Simulations of a Passive Part of the Testing Combustion Facility*, Chemical Engineering Transactions, 2021, 88, 625–630. ISSN 2283-9216.

[4] Thornton, C. and Ning, Z., *A theoretical model for the stick/bounce behaviour of adhesive, elastic-plastic spheres*, Powder Technology. 1998, 99(2), 154–162. ISSN 0032-5910.

[5] ANSYS, Inc., *Ansys® Fluent, Release 21.2, Help System, Fluent Theory Guide*, ANSYS, Inc, 2021.

[6] Lee, B. E., Fletcher, C. A. J., Shin, S. H., and Kwon, S. B., *Computational study of fouling deposit due to surface-coated particles in coal-fired power utility boilers*, Fuel, 2002, 81(15), 2001–2008. ISSN 0016-2361.

[7] Wacławiak, K., and Kalisz, S., *A practical numerical approach for prediction of particulate fouling in PC boilers*, Fuel, 2012, 97, 38–48. ISSN 0016-2361.

[8] Li, J., Du, W., and Cheng, L., *Numerical simulation and experiment of gas-solid two phase flow and ash deposition on a novel heat transfer surface*, Applied Thermal Engineering, 2017, 113, 1033–1046. ISSN 1359-4311.

[9] Brach, R. M. and Dunn, P. F., *A Mathematical Model of the Impact and Adhesion of Microspheres*, Aerosol Science and Technology, 1992, 16(1), 51–64. ISSN 0278-6826.

[10] Hansen, S. B., Jensen, P. A., Frandsen, F. J., Sander, B., and Glaborg, P., *Mechanistic Model for Ash Deposit Formation in Biomass Suspension Firing. Part 1: Model Verification by Use of Entrained Flow Reactor Experiments*, Energy & Fuels, 2017, 31(3), 2771–2789. ISSN 0887-0624.

[11] Losurdo, M., Spliethoff, H. and Kiel, J., *Ash deposition modeling using a visco-elastic approach*, Fuel, 2012, 102, Special Section: ACS Clean Coal, 145–155. ISSN 0016-2361.

[12] Sugawara, A., and Yoshizawa, Y., *An Experimental Investigation on the Thermal Conductivity of Consolidated Porous Materials*, Journal of Applied Physics, 1962, 33(10), 3135–3138. ISSN 1089-7550.

[13] Yagi, S., and Kunii, D., *Studies on effective thermal conductivities in packed beds*, AIChE Journal, 1957, 3(3), 373–381. ISSN 1547-5905.

[14] Westwood, A. R. C., and Hitch, T. T., *Surface Energy of {100} Potassium Chloride*, Journal of Applied Physics, 1963, 34(10), 3085–3089. ISSN 1089-7550.

[15] Kær, S. K., Rosendahl, L. A., and Baxter, L. L., *Towards a CFD-based mechanistic deposit formation model for straw-fired boilers*, Fuel, 2006, 85(5), 833–848. ISSN 0016-2361.

[16] Sommerfeld, M., and Huber, N., *Experimental analysis and modelling of particle-wall collisions*, International Journal of Multiphase Flow, 1999, 25(6), 1457–1489. ISSN 0301-9322.

[17] Xie, J., Dong, M., Li, S., Mei, Y., and Shang, Y., *An experimental study of fly ash particle oblique impact with stainless surfaces*, Journal of Aerosol Science, 2018, 123, 27–38. ISSN 0021-8502.

[18] Weber, R., Schafer-Mancini, N., Mancini, M., and Kupka, T., *Fly ash deposition modelling: Requirements for accurate predictions of particle impaction on tubes using RANS-based computational fluid dynamics*, Fuel, 2013, 108, 586–596. ISSN 0016-2361.

[19] Linstrom, P.J., and W.G. Mallard, Eds., *NIST Chemistry WebBook, NIST Standard Reference Database Number 69*, National Institute of Standards and Technology, Gaithersburg MD, 20899, DOI: doi.org/10.18434/T4D303.

[20] Verein Deutscher Ingenieure, *VDI Heat Atlas*, 2010, Springer-Verlag, Berlin/Heidelberg, Germany, 1585p, ISBN 978-3-540-77876-9.

[21] Raclavská, H., Corsaro , A., Hartmann-Koval, S., and Juchelková, D., *Enrichment and distribution of 24 elements within the sub-sieve particle size distribution ranges of fly ash from wastes incinerator plants*, Journal of Environmental Management, 2017, 203, Environmental management as a pillar for sustainable development, 1169–1177. ISSN 0301-4797.

[22] Wang, F.-L., He, Y.-L., Tong, Z.-X., and Tang, S.-Z., *Real-time fouling characteristics of a typical heat exchanger used in the waste heat recovery systems*, International Journal of Heat and Mass Transfer, 2017, 104, 774–786. ISSN 0017-9310.